Rectification of polymer translocation through nanopores by nonchiral and chiral active particles

Zahra Fazli [1,2,*] and Ali Naji [1,†]

[1]*School of Nano Science, Institute for Research in Fundamental Sciences (IPM), Tehran 19538-33511, Iran*
[2]*School of Physics, Institute for Research in Fundamental Sciences (IPM), Tehran 19538-33511, Iran*

We study translocation of a flexible polymer chain through a membrane pore under the influence of active forces and steric exclusion using Langevin dynamics simulations within a minimal two-dimensional model. The active forces on the polymer are imparted by nonchiral and chiral active particles that are introduced on one side or both sides of a rigid membrane positioned across the midline of a confining box. We show that the polymer can translocate through the pore to either side of the dividing membrane in the absence of external forcing. Translocation of the polymer to a given side of the membrane is driven (hindered) by an effective pulling (pushing) exerted by the active particles that are present on that side. The effective pulling results from accumulation of active particles around the polymer. This crowding effect signifies persistent motion of active particles causing prolonged detention times for them close to the confining walls and the polymer. The effective pushing that hinders the translocation, on the other hand, results from steric collisions that occur between the polymer and active particles. As a result of the competition between these effective forces, we find a transition between two rectified *cis*-to-*trans* and *trans*-to-*cis* translocation regimes. This transition is identified by a sharp peak in the average translocation time. The effects of active particles on the transition is studied by analyzing how the translocation peak is regulated by the activity (self-propulsion) strength of these particles, their area fraction, and chirality strength.

I. INTRODUCTION

Micro- and nanoscale active particles appear in a wide range of living and artificial systems from microorganisms such as bacteria and algae to nano- and microrobots and synthetic Janus particles [1–3]. They often exhibit self-propelled translational motion in liquid media. This motion is caused by specific internal mechanisms that make use of the ambient free energy. These mechanisms include, e.g., ciliary or flagellate organelles as in the case of microorganisms and phoretic forces from autocatalytic surface reactions in the case of Janus particles. Active particles can display fascinating collective properties and self-assembled structures that cannot be understood within the framework of equilibrium physics [4–8]. As a particular example, self-assembled colloidal chains with directed motion can be realized using, e.g., electrohydrodynamic convection rolls in nematic liquid crystals [9], imbalanced electrostatic interactions in systems of metal-dielectric Janus colloids [10], and hydrodynamic interactions due to phoretic flows produced around catalyst-coated colloids linked as a chain [11].

Theoretical and computational models of active chains and filaments have been explored in a growing number of recent works [12–17]. Biological filaments such as F-actin and microtubules in the presence of motility assays (e.g., molecular motors) and also active liquid crystals (active nematics) [18–22] can be modeled as semiflexible polar active chains being tangentially propelled [23,24]. A computationally suitable model of active polymers is that of harmonically linked active Brownian beads that move in two spatial dimensions (2D) [25,26]. Various aspects of active polymers both in 2D and 3D have recently been studied, including chain (hydro)dynamics and diffusivity in viscous and viscoelastic media [27–32], enhanced diffusion [33], coil-globule transition, and shape deformations [34,35] as well as relaxation under imposed shear, shear-induced alignment, and shear thinning [36,37].

Another emerging scenario involves *passive* polymer or filaments suspended in a bath of *active* Brownian particles. The bath activity has been shown to significantly alter conformational statistics and elastic properties of such polymers [38–40]. In this context, a number of peculiar properties, e.g., atypical swelling and looping of flexible filaments, have been reported and bath activity has been shown to cause modulational instability [41,42].

Active forces have also been considered in the context of polymer translocation through nanopores in a dividing membrane [43–45]. The latter has been a major area of interest in soft matter physics [46–56] due to the significance of polymer translocation in important biological and technological applications, including viral DNA ejection [57,58], translocation of single- and double-stranded DNA through α-hemolysin and solid-state nanopores [59,60], and DNA sequencing [61,62].

In recent studies of polymer translocation in active media, effective pulling and pushing forces due to accumulation of active particles around the polymer have been shown to be responsible for nonmonotonic dependence of translocation

_____

*Corresponding author: z.fazli@ipm.ir
†a.naji@ipm.ir

024602-1

time on particle activity and area fraction [43]. The presence of self-propelled rods in one side of the dividing membrane [44] has, on the other hand, been found to facilitate the translocation by inducing a net force on the polymer, engendering a scaling property for the average translocation time as a function of rod length and self-propelling force. Effect of active crowder size on the polymer translocation has also been examined [45], demonstrating that crowders of intermediate size are most favorable for translocation in the case of externally forced (biased) translocation.

In this paper, we also consider polymer translocation through a membrane pore in the presence of active particles and no external forcing (unbiased translocation) but, as a way of extending previous works, we assume that active particles can be either nonchiral or chiral and may be present, with different activity strengths (or Péclet numbers), on one side or both sides of the dividing membrane. The translocation time is computed via Langevin dynamics simulations (in a 2D setting similar to Refs. [43–45]), starting from an initial state where the middle polymer bead is positioned within the pore.

While in the absence of active particles, polymer translocation into either side of the membrane is expectedly found to be equally likely, we show that rectified translocation occurs by introducing active particles on one side or both sides of the membrane. By mapping out parametric "phase" diagrams (based, e.g., on active-particle Péclet numbers, area fractions and chirality), we identify two different regimes of *cis*-to-*trans* and *trans*-to-*cis* rectification. We show that, at the transition boundary between these two regimes, the translocation time exhibits a sharp peak and, hence, the process becomes excessively slow. We show that the transition is produced by the interplay between effective pulling and pushing forces experienced by the polymer. When active particles are chiral, we find a nonmonotonic dependence of the transition point on their chirality strength.

The organization of the paper is as follows. We introduce our model and methods in Sec. II and discuss the baseline case of translocation in the presence of passive particles in Sec. III A. We explore the cases where active particles are present on the *cis* side [case (i)] and both on the *cis* and *trans* sides [case (ii)] in Secs. III B-III D, respectively. The paper is concluded in Sec. IV.

II. MODEL AND METHODS

Our model consists of a single polymer chain comprising N passive beads with diameter σ and mass m_0. The beads are linked linearly via finitely extensible nonlinear elastic (FENE) bonds that are defined through the stretching pair interaction energy [63],

$$U_{\text{FENE}}(r_{ij}) = -\frac{kb_0^2}{2} \ln\left[1 - \left(\frac{r_{ij}}{b_0}\right)^2\right], \qquad (1)$$

for $r_{ij} < b_0$ and $U_{\text{FENE}} = 0$ otherwise. Here $b_0 = 2\sigma$ is the maximal bond stretching length, k is the bond elastic constant and $r_{ij} = |\mathbf{r}_i - \mathbf{r}_j|$ is the distance between consecutive beads labeled by i and $j = 1, \ldots, N$ for which $|i - j| = 1$. The chain is thus fully flexible and has no bending stiffness. The beads also interact sterically among themselves via the
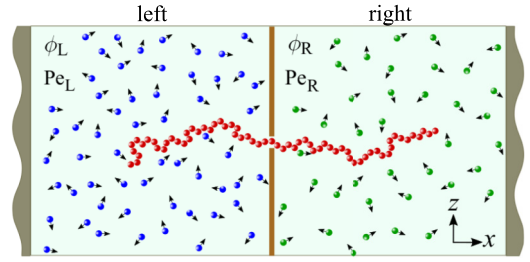

FIG. 1. Schematic view of a passive flexible polymer translocating through a membrane nanopore in the presence of active particles. The particles can be present either on one side of the membrane at area fraction ϕ and Péclet number Pe (not shown) or on both sides of the membrane with left (right) area fraction ϕ_{L} (ϕ_{R}) and Péclet number Pe$_{\text{L}}$ (Pe$_{\text{R}}$).

Weeks-Chandler-Andersen (WCA) pair potential [64]

$$U_{\text{WCA}}(r_{ij}) = 4\varepsilon\left[\left(\frac{\sigma}{r_{ij}}\right)^{12} - \left(\frac{\sigma}{r_{ij}}\right)^6 + \frac{1}{4}\right] \qquad (2)$$

for $r_{ij} < 2^{1/6}\sigma$ and $U_{\text{WCA}} = 0$ otherwise. Here ε and $2^{1/6}\sigma$ are the interaction strength and range, and r_{ij} here is the distance between any arbitrary pair of beads.

The polymer is suspended in a continuum solvent and translocates through a circular nanopore of diameter 2σ designated in a thin, rigid and impermeable membrane of thickness σ; see Fig. 1. The system also contains active Brownian particles, self-propelling due to constant self-propulsive (active) forces of magnitude F_0. For simplicity, we assume that the active particles have the same size and mass as the polymer beads (in the overdamped regime to be considered here, the particle mass becomes obsolete) and that they interact among themselves and with the polymer beads via the same WCA potential as in Eq. (2). All particles are constrained to the x-z plane within a rectangular box of dimensions L_x and $L_z = L_x/2$ in the x and z directions, respectively. Also, the dividing membrane is positioned in the middle of the box and the nanopore at the center of the membrane (Fig. 1).

The system is studied under two cases: Case (i), where active particles are present only on *one* side of the dividing membrane and no particle is present on the other side, and case (ii), where active particles are present on both sides of the membrane with different activity strengths and area fractions (see below). In case (i), we conventionally assume that the particles are present on the left side of the dividing membrane which we identify later as the *cis* side. The cases of passive particles are treated as special cases in (i) and (ii) particle activity is set to zero.

The translational dynamics of active particles are described by the Langevin equation [65]

$$m_0\ddot{\mathbf{r}}_i = F_0\hat{\mathbf{u}}_i - \frac{\partial U}{\partial \mathbf{r}_i} - \gamma_{\text{tr}}\dot{\mathbf{r}}_i + \sqrt{2\gamma_{\text{tr}}k_{\text{B}}T}\,\boldsymbol{\eta}_i(t), \qquad (3)$$

where $\mathbf{r}_i$ is the position of the ith active particle and $\hat{\mathbf{u}}_i$ is its orientation vector which is parametrized by an orientation angle φ_i relative to the x axis, $\hat{\mathbf{u}}_i = (\cos\varphi_i, \sin\varphi_i)$. Also U is the total energy obtained from the sum of all steric and elastic pair interactions as described above, and $k_{\text{B}}T$ is the ambient

thermal energy with k_B being the Boltzmann constant and T the temperature.

For the polymer beads, we use the same dynamical equation as (3) but with $F_0 = 0$ as the beads are modeled as passive Brownian particles (the polymer dynamics thus conforms to the Rouse model [66]). In Eq. (3), γ_{tr} is the single-particle (bulk) translational friction coefficient of the particles and the (thermal) noise terms are assumed to follow Gaussian distributions with mean $\langle \eta_i(t) \rangle = 0$ and two-point correlators $\langle \eta_i^\alpha(t) \eta_j^\beta(t') \rangle = \delta_{ij} \delta_{\alpha\beta} \delta(t - t')$ where $\alpha, \beta = x, z$ represent the Cartesian components. For the active particles, dynamics of the orientation vector is modeled through the equation [65]

$$\dot{\varphi}_i = \omega + \sqrt{\frac{2k_B T}{\gamma_{rot}}} \zeta_i(t), \tag{4}$$

where ω is the intrinsic angular velocity of active particles which is nonzero only in the case of chiral particles, γ_{rot} is their (bulk) rotational friction coefficient, and the noise term satisfies $\langle \zeta_i(t) \rangle = 0$ and $\langle \zeta_i(t) \zeta_j(t') \rangle = \delta_{ij} \delta(t - t')$.

A. Dimensionless quantities

In our forthcoming analysis, we fix the scale of energy as $\varepsilon = k_B T$ and choose σ and $\tau_0 = \sigma\sqrt{m_0/\varepsilon}$ as the reference scales for units of length and time. Hence, e.g., the rescaled distance is defined as $\tilde{r} = r/\sigma$, where applicable, and the average polymer translocation time, to be denoted by τ, is expressed in rescaled form as $\tilde{\tau} = \tau/\tau_0$.

The activity of self-propelling particles is characterized by the corresponding Péclet number (which may interchangeably refer to as the activity strength); i.e.,

$$\text{Pe} = \frac{\sigma F_0}{k_B T} = \frac{\sigma v_0}{D_{tr}}. \tag{5}$$

The second equality here follows from the definition of particle self-propulsion speed $v_0 = F_0/\gamma_{tr}$ and Einstein's relation for particle translational diffusivity $D_{tr} = k_B T/\gamma_{tr}$. As defined, Pe measures the importance of particle self-propulsion relative to (Brownian) translational diffusion. The chirality strength of active particles can be measured in terms of the dimensionless chirality strength,

$$\Gamma = \omega \tau_0. \tag{6}$$

With no loss of generality, we take $\Gamma > 0$; i.e., chiral active particles are assumed to perform persistent counterclockwise rotation of angular velocity $\omega > 0$.

B. Simulation methods

To obtain the translocation time of the polymer chain through the pore as a function of system parameters, we solve Eqs. (3) and (4) numerically using the ESPResSo package [67] and by employing the velocity Verlet algorithm. In our numerical implementation, the active particles and polymer beads are modeled as three-dimensional objects that are constrained to a 2D plane which is bounded in a rectangular simulation box of aforementioned side lengths L_x and L_z. We impose periodic boundary conditions in the z direction and confine the system in the x direction by placing planar rigid walls at $x = 0$ and L_x. The walls and the membrane are

modeled as fixed surfaces and the interactions between them and active particles and the polymer beads are modeled by the same WCA potential as in Eq. (2), with interaction strengths ε taken to be sufficiently large to ensure wall and membrane impermeability.

We start the simulations from an initial state where the middle polymer bead is manually fixed inside the pore and the self-propulsive forces are turned off ($F_0 = 0$) for all particles as the system is equilibrated for 10^6 time steps before the self-propulsive forces are switched on and the middle bead is concurrently released. The simulation time step is chosen in such a way that it remains much smaller than the smallest physically relevant timescale of the system; see Appendix for further details. The translocation time is defined as the time taken (from the moment of release) for either of the polymer end beads to pass through the pore [68]. Each data point in our upcoming plots is obtained by averaging over 100 independent runs with error bars determined accordingly.

C. Choice of parameter values

In our simulations, we have fixed $N = 65$, $L_x/2 = L_z = 50\sigma$, $k = 70k_B T/\sigma^2$, $\gamma_{tr} = 10m_0/\tau_0$, $\gamma_{rot} = 10m_0\sigma^2/\tau_0$ and vary other system parameters within a range representative values; i.e., $\text{Pe} = 0.5 - 10$, $\phi = 0.1 - 0.3$, $\Gamma = 0.05 - 0.7$. These can be mapped to a wide range of realistic parameter values as discussed in Appendix.

For case (i), Secs. III B and III C, the number of active particles is denoted by N_a, and by neglecting the relatively small area occupied by the membrane, their area fraction is defined as $\phi = \pi N_a \sigma^2/(2L_x L_z)$. For case (ii), Sec. III D, we denote the number of active particles on the left and right sides of the membrane by $\{N_{a,L}, N_{a,R}\}$, their Péclet numbers by $\{\text{Pe}_L, \text{Pe}_R\}$, and their area fractions by $\{\phi_L, \phi_R\}$, respectively. In these cases, we change the number of particles in the range $N_a, N_{a,L}, N_{a,R} = 333-1000$, according to the chosen area fraction. In case (ii), and for the sake of simplicity, we only consider nonchiral active particles to reduce the number of system parameters.

As the focus of our study will be on the role of particle activity, chirality, and crowding, we fix the number of polymer beads ($N = 65$) and only vary the Péclet number, chirality strength, and area fraction of active particles throughout of our analysis. Further numerical details are provided in Appendix.

III. RESULTS

A. Translocation with passive particles

Before proceeding with the discussion of our results for the case of active particles, we consider the baseline situation where polymer translocation occurs in the presence of passive Brownian particles ($\text{Pe} = 0$, $\Gamma = 0$) confined to the left side of the membrane. In this case, the passive particles consistently drive out the polymer from their respective (left) compartment to the other (right) side of the dividing membrane, in agreement with previous works [69,70]. The translocation time depends on the area fraction of the passive bath ϕ and is shortened as ϕ is increased; see the inset of Fig. 2(a). We take this rectified translocation transpiring in
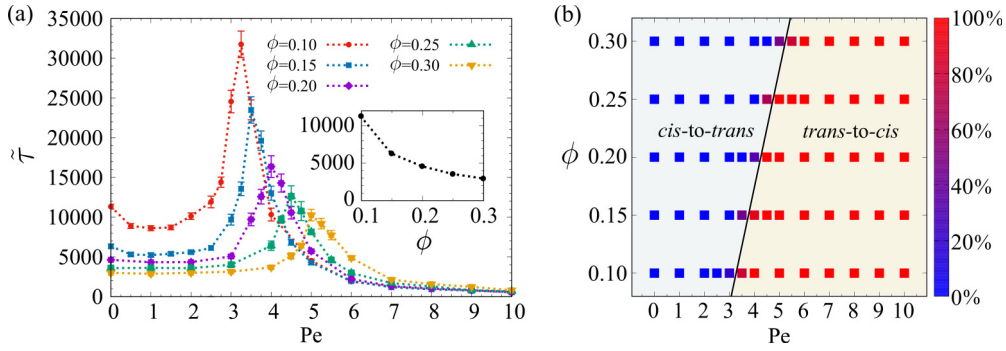
FIG. 2. (a) Main set: Rescaled average translocation time $\tilde{\tau}$ of the polymer in the presence of active particles on the *cis* side of the dividing membrane as a function of Péclet number Pe and at fixed area fraction ϕ for active particles as indicated on the graph. Inset: Translocation time when the bath particles are passive as a function of area fraction ϕ. Symbols are simulation data and dotted curves are guides to the eye. (b) Percentage of translocation events into the *cis* side of the membrane in the Pe-ϕ plane. Color-coded symbols are simulation data and the black line is the boundary between the two indicated regimes.

the presence of passive particles in the left compartment as the *reference cis*-to-*trans* process. We thus identify the left side of the membrane as the *cis* side, a designation that we shall use throughout our discussions of active particles in the following sections as well (note that this designation is different from those in Refs. [43,44] where the compartment with active particles is identified as the *trans* side).

It is also worth noting that the foregoing passive translocation is driven by an effective pushing that stems from thermally induced steric collisions between monomers and the Brownian bath particles, as such collisions impart repulsive WCA forces on the polymer. This reflects the baseline role of thermal fluctuations and the predominantly entropic origin of translocation process when active forces are absent. We shall return to this point later when activity of bath particles is turned on.

B. Nonchiral active particles ($\Gamma = 0$) on the *cis* side

1. Effects of activity strength

In the main set of Fig. 2(a), the rescaled average translocation time $\tilde{\tau}$ of the polymer in the presence of nonchiral ($\Gamma = 0$) active particles on the *cis* side is plotted as a function of the Péclet number Pe for different fixed values of active particle area fraction ϕ. As seen, at sufficiently small Pe, the translocation time remains nearly unchanged relative to its reference value at Pe = 0 albeit with a shallow minimum that appears for the cases of small area fraction $\phi \lesssim 0.15$. The relatively small drop in the translocation time in this case indicates that the weak activity of bath particles tends to enhance the *cis*-to-*trans* translocation, signifying the increased role of collision forces that drive out the polymer from the *cis* side where the particles are present. The situation changes as the Péclet number is increased and the translocation time rapidly increases to a peak value at an intermediate value of Pe$_*(\phi)$ before it falls off, tending to zero as Pe is further increased. This nonmonotonic behavior can be linked to active-particle crowding around the polymer chain at large Pe as we discuss further below and in Sec. III B 3.

In Fig. 2(b), the percentage of chain translocation events into the *cis* side of the membrane is plotted in the Pe-ϕ

parameter space. Recall that, in the present context, no external forcing is present and the chain is not barred from translocating into either side of the membrane. In the color-coding of the plot, blue (red) indicates that the chain consistently escapes from the active *cis* side (*trans* side) into the *trans* side (*cis* side) and the spectrum of colors in between indicate the mixed cases where both processes occur with the given probability on the side bar. As inferred from the plot, at sufficiently small Pe, the polymer can always evade the active particles and enter the *trans* side; while, at sufficiently large Pe, the polymer is always captured back into the active *cis* side. For practical purposes, we define the *cis*-to-*trans* (*trans*-to-*cis*) regime as the region of parameters where the chain translocates with probability $> 50\%$ into the *trans* (*cis*) side. As seen in Fig. 2(b), the transition between these two regimes occurs rapidly, i.e., over a narrow region (purple symbols) over the Pe-ϕ plane around the boundary line between the said regimes (solid black line). The boundary line Pe = Pe$_*(\phi)$ coincides with the peak location in Fig. 2(a) where translocation events to *cis* and *trans* sides become equally likely. Our results in Fig. 2(b) thus imply that, except for the narrow transition region noted above, the translocation is always *rectified*, as virtually all translocation events proceed either in *cis*-to-*trans* or *trans*-to-*cis* direction.

It is also useful to examine typical snapshots of the system from the simulations. In Fig. 3, we simulated snapshots for three values of the Péclet number Pe = 1, 5, and 10. For small Pe, the active particles are generally found to have a nearly even distribution in the box, while they become increasingly more populated around the polymer chain as well as the diving membrane and the confining side wall of the compartment at larger Pe (recall that periodic boundary conditions are imposed on the top and bottom edges of the simulation box). The accumulation of active particles in the proximity of confining walls and other external objects (including flexible chains [42]) is an intrinsically nonequilibrium effect that manifests the prolonged local detention time of active particles near interfacial boundaries; an effect that is known to result directly from the persistent self-propelled motion of the particles [71,72] and which we shall elaborate on further in Sec. III B 3.
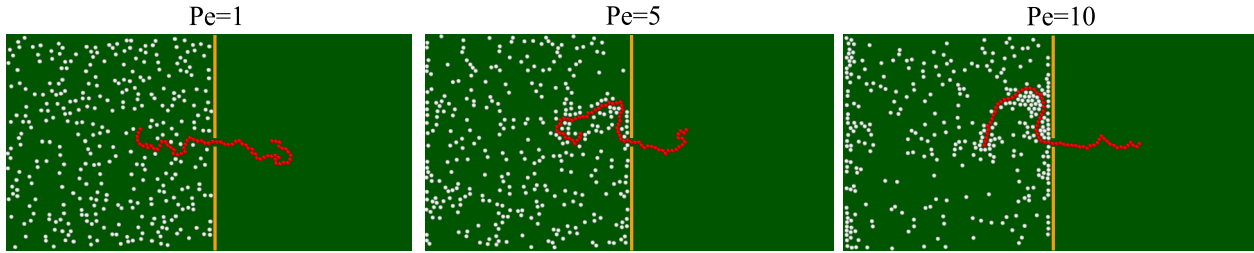
FIG. 3. Typical simulation snapshots for translocation of the polymer chain in the presence of active particles on the *cis* side of the dividing membrane for Péclet numbers Pe = 1, 5, and 10 and fixed area fraction $\phi = 0.1$ of active particles.

The peaked translocation time in Fig. 2(a) can in fact be attributed to an effective pulling force that is produced on the polymer chain due to increased crowding of active particles around the polymer. In other words, this pulling effect tends to oppose the baseline pushing which is experienced by the polymer from thermally induced steric collisions on the *cis* side (Sec. III A), hence resulting in the slow-down of the *cis*-to-*trans* translocation at small to intermediate values of Péclet number. The *cis*-to-*trans* regime indicated in the "phase" diagram of Fig. 2(b), i.e., Pe < Pe$_*(\phi)$, can nevertheless be viewed as the regime of parameters where thermal fluctuation effects are still significant and active pulling is not strong enough to modify the qualitative aspects of the translocation process relative to the passive case (note, however, that the thermal and active contributions in this regime are intertwined and cannot in general be disentangled, especially because the rotational noise term in Eq. (4) is an essential ingredient of active Brownian particles [73] that we have used in our model).

As the Péclet number is further increased, i.e., for Pe > Pe$_*(\phi)$, the aforesaid wall accumulation and crowding effect become dominant (compare the snapshots with Pe = 5 and 10 in Fig. 3). Hence, the active pulling back into the *cis*-compartment dominates and triggers rapid *trans*-to-*cis* translocation of the polymer, also explaining the rapid drop in translocation time beyond the peak location in Fig. 2(a). The *trans*-to-*cis* regime in Fig. 2(b) thus signifies the activity-dominated part of the parameter space and corroborates the

fact that polymer translocation can be rectified (or reversed) under the influence of active agents.

2. Effects of area fraction

Figure 2(a) also indicates the effects of area fraction ϕ for active particles; i.e., the peak translocation time has a relatively large value at small ϕ and it decreases as ϕ is increased. It also shows that the locus of the peak shifts to larger Péclet numbers Pe as ϕ is increased. This shift can also be inferred from the transition line in Fig. 2(b) which shows that, at larger ϕ, the transition between *cis*-to-*trans* and *trans*-to-*cis* regimes occurs at larger Pe. This effect reflects the fact that, even as the effective active pulling of the polymer is strengthened at larger area fractions of active particles on the *cis* side, the pushing effect due to steric collisions of particles with the polymer also grows in strength; hence, necessitating even larger Péclet numbers to induce *trans*-to-*cis* translocation.

3. Activity-induced steric layering

For a better understanding of the role played by active forces in the translocation of the polymer chain, the distribution of active particle distance from the chain, $\mathcal{P}(\tilde{r}_{\rm dist})$, is plotted in Fig. 4 for different values of Péclet numbers. This quantity is defined as the probability of finding an active particle at a specified distance, $\tilde{r}_{\rm dist}$, from the polymer chain where $\tilde{r}_{\rm dist}$ is the distance between the active particles and the nearest monomer of the chain ($\tilde{r}_{\rm dist}$ is obtained at every time
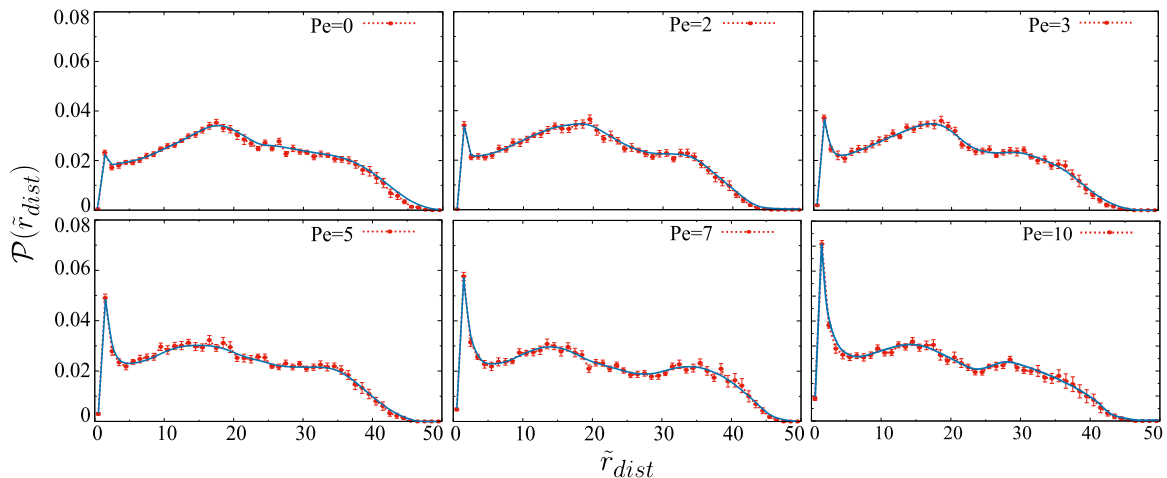

FIG. 4. Distance distribution $\mathcal{P}(\tilde{r}_{\rm dist})$ of active particles from the polymer chain, as defined in the text, for different values of particle Péclet numbers at fixed area fraction $\phi = 0.2$.
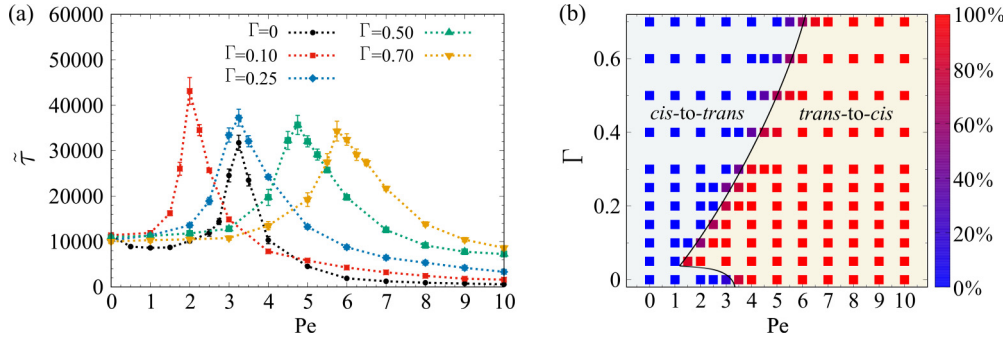
FIG. 5. (a) Rescaled average translocation time $\tilde{\tau}$ of the polymer in the presence of chiral active particles on the *cis* side of the dividing membrane as a function of Péclet number Pe and at fixed chirality strength Γ for active particles as indicated on the graph. Symbols are simulation data and dotted curves are guides to the eye. (b) Percentage of translocation events into the *cis* side of the membrane in the Pe-Γ plane. Color-coded symbols are simulation data and the black line is the transition boundary between the two indicated regimes. In both panels, the area fraction of active particles is fixed as $\phi = 0.1$.

step by evaluating distances between each one of the active particles and all of the chain monomers and by designating the smallest of these distances as $\tilde{r}_{\text{dist}}$ for the active particle in question). In the simulations, we compute $\mathcal{P}(\tilde{r}_{\text{dist}})$ using the relation

$$\mathcal{P}(\tilde{r}_{\text{dist}}) = \frac{1}{N_a} \langle n(\tilde{r}_{\text{dist}}) \rangle, \tag{7}$$

where N_a is the number of active particles on the *cis* side of the membrane, $n(\tilde{r}_{\text{dist}})$ is the number of active particles found at the distance $\tilde{r}_{\text{dist}}$ from the chain as defined above, and $\langle \cdots \rangle$ is the time and ensemble averaging used in the simulations (Sec. II B).

As seen in Fig. 4, for the passive bath (Pe = 0), the most probable distance of the particles from the polymer is positioned somewhere in the bulk of the box, signifying steric repulsions experienced by the particles due to large-amplitude fluctuations of the polymer chain. In the case of active particles with sufficiently large Péclet numbers, see the panels for Pe = 3, 5, 7, 10, a sharp peak in $\mathcal{P}(\tilde{r}_{\text{dist}})$ develops at a distance comparable to a single particle size ($\tilde{r}_{\text{dist}} \simeq 1$). This indicates a dense layer of active particles accumulate in the immediate vicinity of the polymer chain, corroborating our discussions of the crowding effect in Sec. III B 1. The aforementioned panels in Fig. 4 also reveal two broad peaks at larger values of $\tilde{r}_{\text{dist}}$. These are also indicative of consecutive layering of active particles further away from the polymer. While the amplification of the small-distance peak reflects dominant activity-induced particle accumulation near the chain, these latter large-distance peaks indicate weakened activity effects, as expected, and their signature may also be discerned from the panel for passive particles (Pe = 0). The nonequilibrium layering of active particles results from the interplay between particle tendency for accumulation near external boundaries and steric interparticle repulsions and can be demonstrated most clearly in the case of rigid and permeable inclusions immersed in an active bath [74–77].

C. Chiral active particles ($\Gamma \neq 0$) on the *cis* side

We proceed by considering the case of chiral active particles that are present only on the *cis* side of the dividing

membrane. Being representative of intrinsic rotational motion, particle chirality can lead to a host of different phenomena in confined systems [77–82]. To our knowledge, chirality effects have remained unexplored in the context of polymer translocation.

In Fig. 5(a), rescaled average translocation time $\tilde{\tau}$ of the polymer chain in the presence of chiral active particles with area fraction $\phi = 0.1$ on the left side of the membrane is plotted as a function of the particle Péclet number Pe and for different fixed chirality strengths Γ. As seen, the translocation time peaks at an intermediate value of Pe$_*(\Gamma)$, indicating a transition similar to the one discussed in Sec. III B. Figure 5(a) also indicates that the peak location in the plot Pe$_*$ varies nonmonotonically with Γ. For small $\Gamma < 0.25$, the plotted curves are shifted to the left when compared with the nonchiral case ($\Gamma = 0$). For $\Gamma = 0.25$, the peak location appears to coincide with that in the nonchiral case; i.e., Pe$_* = 3.25$ (compare blue and black data points). For larger values of chirality strength, $\Gamma > 0.25$, the peak location in the plot is shifted to the right relative to the nonchiral case.

Figure 5(b) shows a more comprehensive view of our results by depicting the percentage of *cis*-to-*trans* and *trans*-to-*cis* translocation events in the Pe-Γ plane at fixed area fraction of active particles, $\phi = 0.1$. In analogy to Fig. 2(b), the two regimes of rectified translocations are separated by a narrow transition region (purple symbols). The transition curve Pe = Pe$_*(\Gamma)$ is indicated by the black curve which again corresponds to the loci of peaks in Fig. 5(a) where the *cis*-to-*trans* and *trans*-to-*cis* translocations occur with equal likelihoods. Unlike the case in Fig. 2(b), the transition curve here shows a cusp, reflecting the aforementioned nonmonotonic behavior of Pe$_*(\Gamma)$ as a function of Γ. It is also evident from the "phase" diagram of Fig. 5(b) that, when the Pe is adjusted in the region values around the cusp (i.e., $1 \lesssim$ Pe $\lesssim$ 3.25 in the figure) and Γ is increased from zero, the system can show a *re-entrant* behavior [83] by proceeding from the *cis*-to-*trans* regime into the *trans*-to-*cis* regime and again into the *cis*-to-*trans* regime at larger values of Γ.

Another interesting aspect of our results in Fig. 5(a) is that the translocation times (especially its peak value) is increased for chiral active particles relative to the nonchiral ones (compare black data with other colored data). This effect originates
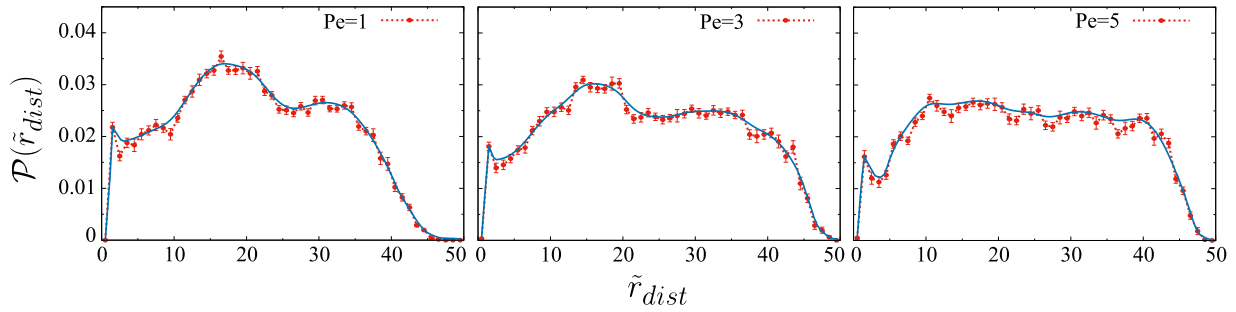
FIG. 6. Distance distribution $\mathcal{P}(\tilde{r}_{\text{dist}})$ of chiral active particles from the polymer chain, as defined in the text, for different values of particle Péclet numbers at fixed chirality strength $\Gamma = 0.2$ and fixed area fraction $\phi = 0.1$.

from the fact that particle chirality weakens the persistent motion of active particles as the direction of particle self-propulsion is continuously reoriented by the angular velocity ω in Eq. (4). This suppresses the boundary accumulation of active particles [77,82], also their crowding around the polymer. Consequently, the effective pulling induced by particle activity (Sec. III B) is also weakened, leading to slower translocation overall. In other words, one requires a larger Péclet number to achieve the same *trans*-to-*cis* translocation time as in the nonchiral case.

The distance distribution $\mathcal{P}(\tilde{r}_{\text{dist}})$ of chiral active particles around the polymer chain is plotted in Fig. 6 for three different values of particle Péclet numbers. As seen, the sharp small-distance peak due to active accumulation of particles near the chain is significantly reduced in comparison with the nonchiral case in Fig. 4, corroborating our foregoing discussion of chirality effects. Also, the spatial distribution of chiral particles becomes increasingly more even as Pe increases. This can be understood by noting that, for a fixed chirality strength Γ, chiral active particles tend to traverse circular trajectories of radius $\sim$Pe$/\Gamma$. This latter quantity becomes large as Pe increases, destroying the steric layering of active particles relative to the nonchiral case in Fig. 4.

D. Active particles on both *cis* and *trans* sides

We now turn to the case of polymer translocation where active (or passive) particles are present on both sides of

the membrane. For simplicity, the active particles are here assumed to be nonchiral. In the main set of Fig. 7(a), we show the rescaled average translocation time when the Péclet number of particles is fixed as Pe$_R = 0, 3, 5$, and 7 in the right (*trans*) compartment, while the Péclet number of particles in the left (*cis*) compartment varies. The area fractions of particles in the said compartments are fixed as $\phi_R = 0.1$ and $\phi_L = 0.2$, respectively. As in case (i), where particles are present only on the *cis* side, the peaks in the plot denote transitions between *cis*-to-*trans* to *trans*-to-*cis* translocations.

The transition curve that separates the two regimes of rectified *cis*-to-*trans* and *trans*-to-*cis* translocations are depicted in the Pe$_R$-Pe$_L$ plane in the inset of Fig. 7(a) (note that the transition region has a small width similar to Figs. 2(b) and 5(b) which is not shown here). As seen, for Pe$_R = 0$ and at low Pe$_L$, including specifically the passive case with Pe$_L = 0$, the polymer translocates into the *trans* side. This is because of the larger area fraction which is chosen for the *cis* compartment $\phi_L > \phi_R$ and also the dominant thermally induced steric collisions that effectively push the polymer into the *trans* side. The corresponding data set in Fig. 7(a) (main set, red symbols with Pe$_R = 0$) shows a shallow minimum at small Pe$_L \sim 1$ similar to Fig. 2(a), indicating that small activity of particles on the *cis* side can partially facilitate translocation of the polymer into the *trans* side. As Pe$_L$ is increased for Pe$_R = 0$, i.e., above Pe$_L \simeq 3.75$, the pulling effect from active particles on the *cis* side dominates and the system enters the *trans*-to-*cis* translocation regime above the separating boundary curve. In
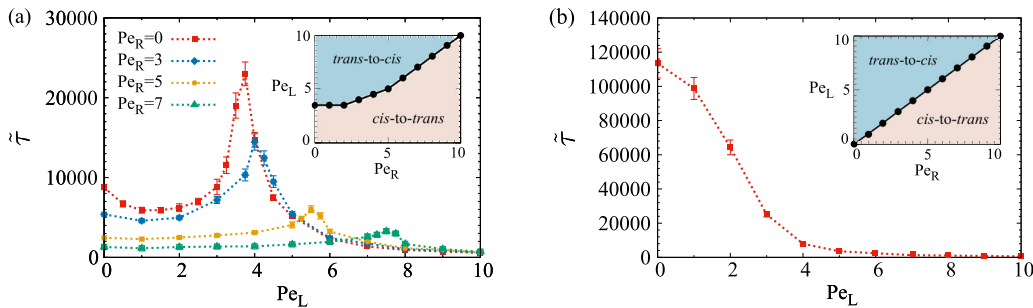

FIG. 7. (a) Main set: Rescaled average translocation time $\tilde{\tau}$ of the polymer with area fractions $\phi_L = 0.2$ and $\phi_R = 0.1$ on the *cis* and *trans* sides of the dividing membrane, respectively, as a function of Péclet number Pe$_L$ of active particles on the *cis* side. The Péclet number Pe$_R$ of active particles on the *trans* side is fixed as indicated on the graph. Inset: The regime of *cis*-to-*trans* and *trans*-to-*cis* translocation in the Pe$_R$-Pe$_L$ plane. (b) Main set: Same as (a) but in the case where area fractions of particles on the two sides are equal $\phi_L = \phi_R = 0.1$ and the Péclet number of particles on the *trans* side Pe$_R = 0$ (passive particles). Inset shows the corresponding "phase" diagrams for matching area fractions as in the main set. In the main sets of panels (a) and (b), symbols are simulation data and curves are guides to the eye.

this regime, the translocation time drops rapidly with Pe_L according to the main set of Fig. 7(a) but it remains nearly independent of Pe_R (note that the different data sets in the main set nearly overlap at sufficiently large Pe_L).

Our results in the inset of Fig. 7(a) also show that the transition between *cis*-to-*trans* and *trans*-to-*cis* regime (i.e., reversal of rectified translocations) can be achieved at all values of Pe_R when Pe_L is varied. By contrast, when Pe_R is varied, such a transition can be achieved only when Pe_L is sufficiently large value; i.e., $Pe_L \gtrsim 3.75$; otherwise, adjusting Pe_R cannot produce a reversal in the rectified *cis*-to-*trans* translocation. This can be understood by noting that, for small Pe_L, the effective pulling of the polymer by active particles on the *cis* side is weak while the polymer is also concurrently pulled into the *trans* side by active particles on that side, especially when Pe_R is increased. This latter point also explains why the *cis*-to-*trans* regime expands upon increasing Pe_R.

One should bear in mind that, in the case under consideration in Fig. 7(a), the area fraction of active particles on the *cis* side is assumed to be larger than the *trans* side. Our results in the inset of the figure, however, show that the transition curve for sufficiently large activity strengths on both sides of the membrane tends to the line $Pe_R = Pe_L$. This indicates that, despite the mismatching area fractions, the effective pulling forces that the polymer experiences from active particles in the two compartments are nearly balanced provided the Péclet numbers are large enough.

To shed further light on the subtle role of area fraction, we consider the case where area fractions of particles on the *cis* and *trans* sides of the dividing membrane are equal $\phi_L = \phi_R = 0.1$. Let us first consider the specialized case where particles on the *trans* side are passive ($Pe_R = 0$); see Fig. 7(b). In this case, the translocation time exhibits no nonmonotonicity as a function of Pe_L and the translocation (occurring here always in *trans*-to-*cis* direction) becomes continually faster ($\tilde{\tau}$ monotonically falls off) as Pe_L is increased. The matching of area fractions on the two sides of the membrane in fact removes the effective pushing mechanism that would drive out the polymer from the *cis* side. In other words, the pushing forces stemming from steric collisions of bath particles with the polymer on the two sides of the membrane essentially offset one another. For this reason, the translocation of the polymer also becomes relatively slow, as one can infer by comparing the maximal value of $\tilde{\tau}$ in Fig. 7(b), main set, with the peak values in Figs. 2(a), 5(a), and 7(a), main set. The inset of Fig. 7(b) shows the overall picture when the particles on the *trans* side are also allowed to be active. As seen, the two *cis*-to-*trans* and *trans*-to-*cis* translocation regimes emerge symmetrically and the transition boundary between them coincides perfectly with the line $Pe_R = Pe_L$ across the entire Pe_R-Pe_L plane. This means that no *cis*-to-*trans* regime will be present for $Pe_R = 0$ with matching *cis* and *trans* area fractions; that is, the maximal translocation time found in the main set of the figure indeed corresponds to the peak or transition point which is here shifted to $Pe_L = 0$, eliminating the *cis*-to-*trans* behavior found in the other case reported in this work. As a result, the reversal of translocation can similarly be achieved by adjusting either of the Péclet numbers Pe_L and Pe_R.

IV. CONCLUDING REMARKS

In this work, we have studied translocation of a flexible polymer chain through a membrane nanopore in the presence of nonchiral and chiral active particles on one side or both sides of the dividing membrane. This is done by performing Langevin dynamics simulations of a well-established minimal model of active particles and flexible polymers in two spatial dimensions. The translocation is studied in the absence of external forcing.

In the cases where active particles are present only on one side of the membrane, which is identified as the *cis* side, we showed that the translocation time exhibits a nonmonotonic behavior as a function of the activity strength (Péclet number) of active particles with a sharp peak appearing at intermediate Péclet numbers where the translocation becomes excessively slow. The peak was shown to indicate a transition between two rectified states of translocation, namely *cis*-to-*trans* and *trans*-to-*cis* translocations. While the former transpires at small Péclet numbers, the latter occurs at large Péclet numbers beyond the peak value. In *cis*-to-*trans* (*trans*-to-*cis*) regime, virtually all translocation events proceed from the *cis* (*trans*) compartment into the *trans* (*cis*) compartment. At the transition, which is shown to occur relatively rapidly (i.e., over a narrow range of Péclet numbers), both translocation events become equally likely as the direction of rectified translocation is reversed. We argued that the *cis*-to-*trans* translocation occurs as a result of dominant thermally induced steric collisions that take place between particles and chain monomer in the *cis* side. This leads to an effective pushing force on the polymer that tends to drive the polymer into the *trans* side. By contrast, the *trans*-to-*cis* translocation is driven by the active crowding of the particles around the polymer (especially, as a dense layer along the chain) which creates an effective force pulling the polymer into the *cis* side. The counterbalance between these mechanisms leads to a slow translocation of the polymer and, hence, the aforesaid peak and the reversal of its rectified translocation.

We have thoroughly examined the behavior of the system for different area fractions and chirality strengths of actives particles and also when active particles can be present on both sides of the membrane. The results are summarized in parametric "phase" diagrams. In the case of chiral particles, our results reveal a nonmonotonic transition boundary between the above-mentioned regimes of translocation with a distinct cusp that emerges in an intermediate interval of Péclet numbers. This indicates a re-entrant behavior, meaning that the translocation can be reversed through two distinct transition points as it goes from the *cis*-to-*trans* regime into the *trans*-to-*cis* regime and again into the *cis*-to-*trans* regime while the chirality strength of active particles is continually increased from zero.

Our model and analysis are based on certain assumptions that can be amended or generalized to enable possible extensions of the study. Some of these can be summarized as follows.

First, the confinement in our model is taken as rectangular box with hard walls in the x direction and periodic boundary conditions in the z direction. It is thus interesting to examine situations where the system is enclosed by hard walls in

all directions and, specifically, when the system is confined in a circular enclosure. In these cases, a larger fraction of active particles would accumulate on the walls than around the polymer itself as compared with the case analyzed in this work. Hence, we expect that the transition boundary, e.g., in Fig. 2(b) shift to the right, expanding the regime of *cis*-to-*trans* translocation. In the case of chiral particles, finite chirality-induced currents are expected to appear on the boundaries [81,82] whose effects on the translocation process remains to be explored.

Second, our study is performed for a fixed length of the translocating polymer. This is done to bring out the effects from the *active-bath parameters*, including particle activity, area fraction and chirality strength that are at the focus of the present work. It is nevertheless important to examine the role of *polymer parameters*, specifically, the role of chain length in future studies. Such an analysis can unravel possible scaling of the translocation time with the chain length in line with similar analyses done for nonactive polymer translocation (see, e.g., Refs. [48,50,51,55,84,85] and references therein) and recently also for active polymer translocation in Ref. [44]. A scaling analysis should provide major insights into the problem complementing what we report through our findings in this work. It would also be interesting to compare possible scaling behaviors of active polymers in the present context with those obtained for passive polymers through thermodynamic approaches [86].

Third, our analysis is focused on the effects that arise when the activity strength (Péclet number) of active bath particles are increased to overwhelm the thermal noise effects. We have also conducted our analysis at fixed temperature. Since we use a dimensionless representation in our simulations by rescaling all units of energy with the ambient thermal energy $k_{\rm B}T$, the effects of temperature cannot (in a strict sense) be probed directly through our implementation and requires a routine reformulation of the rescaling scheme used herein. Yet, the role of thermal fluctuations can still be addressed indirectly through the Péclet number, Pe $= \sigma F_0/(k_{\rm B}T) = \sigma v_0/D_{\rm tr}$, which gives a measure of active particle self-propulsion relative to thermal diffusion; see Eq. (5). Thus, for instance, the effects of increasing T may indirectly be inferred by scanning the "phase" diagrams of Figs. 2(b) and 5(b) in a reverse direction along the Pe axis. This corroborates our discussions in Secs. III A, III B 1, and III D where we argue that polymer translocation in the regime of small Pe is generally dominated by thermal fluctuations in the bath: These fluctuations trigger steric collisions between bath particles and chain monomers, leading to the pushing mechanism responsible for the *cis*-to-*trans* translocation. In summary, while the vertical lines with Pe $= 0$ in the said "phase" diagrams have strict thermal signature, the left sides of the transition boundaries represent regions where thermal fluctuations are still dominant relative to active self-propulsion effects. The situation is reversed on the right side of the transition boundaries.

An in-depth analysis of noise-induced and temperature-dependent effects within the current problem would be an interesting avenue to explore in the future, given the wide range of phenomena known to emerge from noise and thermal fluctuations in the broader context of nonlinear complex systems; see, e.g., Refs. [87–93] and references therein. This task can be done by analyzing other relevant quantities than considered in our study, such as the mean first passage time; also, by generalizing the model to scrutinize possible effects from resonant activation, time-dependent driving forces, detailed polymer-pore interactions, and other phenomena addressed previously in the context of nonactive polymers [94–101].

Finally, we note that the dynamics of the polymer in our model neglects the role of hydrodynamic interactions as it corresponds to the so-called Rouse model [66]. Aside from hydrodynamic interactions (e.g., between active particles, polymer chain and the dividing membrane), one can also investigate the role of chain stiffness and the solvent quality, paving the way for more intriguing scenarios to be studied in the present context.

APPENDIX: FURTHER DETAILS ON THE CHOICE OF PARAMETERS

As noted in Sec. II C, our choices of values for the dimensionless parameters can be mapped to a wide range of actual values in realistic settings. In particular, the range of Péclet numbers used here to explore the system behavior can be achieved through artificial nanoswimmers such as Janus nanoparticles (Pe $\simeq$ 1–3) [102] and platinum-loaded stomatocyte nanomotors (Pe $\simeq$ 1–5) [103]. Our investigated range of particle chirality Γ can also be realized through artificial active particles such as curved self-propelled rods ($|\Gamma| \simeq$ 0.1–0.5) [104,105] and self-assembled rotors ($|\Gamma| \simeq$ 0.1–1) [106].

Finally, we note that the time step in our simulations is fixed as $\Delta t = 10^{-2}\tau_0$. Our inspections reveal negligible effects from the choice of time step when the latter is set at a smaller value such as $5 \times 10^{-3}\tau_0$ (these checks are run on a fewer number of data points than reported in the text due to limitations on our computational resources). This is expected given that the smallest timescale in our model is set by τ_0. For comparison, some of the main physically relevant timescales in our model are $\tau_\sigma = \sigma/v_0$ (which is the time it takes for an active particle to self-propel a distance about its size), $\tau_{\rm tr} = \sigma^2/D_{\rm tr}$, and $\tau_{\rm rot} = 1/D_{\rm rot}$ (which are the translational and rotational diffusion timescales). According to the parameter definitions in Sec. II, one can equivalently express these as $\tau_\sigma = 10\tau_0/$Pe and $\tau_{\rm tr} = \tau_{\rm rot} = 10\tau_0$. Since the Péclet number in our study is varied in the range Pe $= 0.5$–10, τ_σ changes over the range $\tau_\sigma = 1 - 20\,\tau_0$. In other words, the chosen time step $\Delta t = 10^{-2}\tau_0$ remains desirably small relative to the other key timescales probed within our simulations; i.e., $\Delta t = (5 \times 10^{-4} - 10^{-2})\tau_\sigma$ and $\Delta t = 10^{-3}\tau_{\rm tr,rot}$.

[1] E. Lauga and T. R. Powers, Rep. Prog. Phys. **72**, 096601 (2009).

[2] T. Vicsek and A. Zafeiris, Phys. Rep. **517**, 71 (2012).

[3] J. Zhang, B. A. Grzybowski, and S. Granick, Langmuir **33**, 6964 (2017).

[4] C. Bechinger, R. Di Leonardo, H. Löwen, C. Reichhardt, G. Volpe, and G. Volpe, Rev. Mod. Phys. **88**, 045006 (2016).

[5] M. C. Marchetti, J. F. Joanny, S. Ramaswamy, T. B. Liverpool, J. Prost, M. Rao, and R. A. Simha, Rev. Mod. Phys. **85**, 1143 (2013).

[6] F. Jülicher, S. W. Grill, and G. Salbreux, Rep. Prog. Phys. **81**, 076601 (2018).

[7] J. Elgeti, R. G. Winkler, and G. Gompper, Rep. Prog. Phys. **78**, 056601 (2015).

[8] D. Needleman and Z. Dogic, Nat. Rev. Mater. **2**, 17048 (2017).

[9] Y. Sasaki, Y. Takikawa, V. S. R. Jampani, H. Hoshikawa, T. Seto, C. Bahr, S. Herminghaus, Y. Hidaka, and H. Orihara, Soft Matter **10**, 8813 (2014).

[10] J. Yan, M. Han, J. Zhang, C. Xu, E. Luijten, and S. Granick, Nat. Mater. **15**, 1095 (2016).

[11] B. Biswas, R. K. Manna, A. Laskar, P. S. Kumar, R. Adhikari, and G. Kumaraswamy, ACS Nano **11**, 10025 (2017).

[12] G. A. Vliegenthart, A. Ravichandran, M. Ripoll, T. Auth, and G. Gompper, Sci. Adv. **6**, eaaw9975 (2020).

[13] D. Loi, S. Mossa, and L. F. Cugliandolo, Soft Matter **7**, 10193 (2011).

[14] D. Osmanovic and Y. Rabin, Soft Matter **13**, 963 (2017).

[15] J. Denk, L. Huber, E. Reithmann, and E. Frey, Phys. Rev. Lett. **116**, 178301 (2016).

[16] H. Löwen, Europhys. Lett. **121**, 58001 (2018).

[17] C. Abaurrea-Velasco, T. Auth, and G. Gompper, New J. Phys. **21**, 123024 (2019).

[18] Y. Harada, A. Noguchi, A. Kishino, and T. Yanagida, Nature (London) **326**, 805 (1987).

[19] N. Kumar, R. Zhang, J. J. de Pablo, and M. L. Gardel, Sci. Adv. **4**, eaat7779 (2018).

[20] C. A. Whitfield, T. Chandra Adhyapak, A. Tiribocchi, G. P. Alexander, D. Marenduzzo, and S. Ramaswamy, Eur. Phys. J. E **40**, 50 (2017).

[21] P. Srivastava, P. Mishraa, and M. C. Marchetti, Soft Matter **12**, 8214 (2016).

[22] S. P. Thampi, R. Golestanian, and J. M. Yeomans, Europhys. Lett. **105**, 18001 (2014).

[23] R. E. Isele-Holder, J. Elgeti, and G. Gompper, Soft Matter **11**, 7181 (2015).

[24] R. E. Isele-Holder, J. Jäger, G. Saggiorato, J. Elgeti, and G. Gompper, Soft Matter **12**, 8495 (2016).

[25] R. Chelakkot, A. Gopinath, L. Mahadevan, and M. F. Hagan, J. R. Soc. Interface. **11**, 20130884 (2014).

[26] A. Kaiser, S. Babel, B. ten Hagen, C. von Ferber, and H. Löwen, J. Chem. Phys. **142**, 124905 (2015).

[27] A. Laskar and R. Adhikari, Soft Matter **11**, 9073 (2015).

[28] G. Jayaraman, S. Ramachandran, S. Ghose, A. Laskar, M. S. Bhamla, P. B. Sunil Kumar, and R. Adhikari, Phys. Rev. Lett. **109**, 158302 (2012).

[29] R. G. Winkler, J. Elgeti, and G. Gompper, J. Phys. Soc. Jpn. **86**, 101014 (2017).

[30] H. Jiang and Z. Hou, Soft Matter **10**, 1012 (2014).

[31] T. B. Liverpool, A. C. Maggs, and A. Ajdari, Phys. Rev. Lett. **86**, 4171 (2001).

[32] H. Vandebroek and C. Vanderzande, Phys. Rev. E **92**, 060601(R) (2015).

[33] V. Bianco, E. Locatelli, and P. Malgaretti, Phys. Rev. Lett. **121**, 217802 (2018).

[34] S. Das, N. Kennedy, and A. Cacciuto, Soft Matter **17**, 160 (2021).

[35] T. Eisenstecken, G. Gompper, and R. G. Winkler, J. Chem. Phys. **146**, 154903 (2017).

[36] A. Martín-Gómez, G. Gompper, and R. G. Winkler, Polymers **10**, 837 (2018).

[37] R. G. Winkler, Soft Matter **12**, 3737 (2016).

[38] N. Samanta and R. Chakrabarti, J. Phys. A: Math. Theor. **49**, 195601 (2016).

[39] A. Kaiser and H. Löwen, J. Chem. Phys. **141**, 044903 (2014).

[40] J. Harder, C. Valeriani, and A. Cacciuto, Phys. Rev. E **90**, 062312 (2014).

[41] J. Shin, A. G. Cherstvy, W. K. Kim, and R. Metzler, New J. Phys. **17**, 113008 (2015).

[42] N. Nikola, A. P. Solon, Y. Kafri, M. Kardar, J. Tailleur, and R. Voituriez, Phys. Rev. Lett. **117**, 098001 (2016).

[43] M. Pu, H. Jiang, and Z. Hou, J. Chem. Phys. **145**, 174902 (2016).

[44] H. Khalilian, J. Sarabadani, and T. Ala-Nissila, Phys. Rev. Res. **3**, 013080 (2021).

[45] F. Tan, Y. Chen, and N. Zhao, Soft Matter **17**, 1940 (2021).

[46] S. Matysiak, A. Montesi, M. Pasquali, A. B. Kolomeisky, and C. Clementi, Phys. Rev. Lett. **96**, 118103 (2006).

[47] J. M. Polson and A. C. M. McCaffrey, J. Chem. Phys. **138**, 174902 (2013).

[48] T. Sakaue, Phys. Rev. E **76**, 021803 (2007).

[49] K. Luo, T. Ala-Nissila, S.-C. Ying, and R. Metzler, Europhys. Lett. **88**, 68006 (2009).

[50] J. Chuang, Y. Kantor, and M. Kardar, Phys. Rev. E **65**, 011802 (2001).

[51] Y. Kantor and M. Kardar, Phys. Rev. E **69**, 021806 (2004).

[52] J. Sarabadani and T. Ala-Nissila, J. Phys.: Condens. Matter **30**, 274002 (2018).

[53] W. Sung and P. J. Park, Phys. Rev. Lett. **77**, 783 (1996).

[54] M. Muthukumar, J. Chem. Phys. **111**, 10371 (1999).

[55] V. V. Palyulin, T. Ala-Nissila, and R. Metzler, Soft Matter **10**, 9016 (2014).

[56] T. Sakaue, Polymers **8**, 424 (2016).

[57] Z. T. Berndsen, N. Keller, S. Grimes, P. J. Jardine, and D. E. Smith, Proc. Natl. Acad. Sci. USA **111**, 8345 (2014).

[58] M. M. Inamdar, W. M. Gelbart, and R. Phillips, Biophys. J. **91**, 411 (2006).

[59] M. Wanunu, W. Morrison, Y. Rabin, A. Y. Grosberg, and A. Meller, Nat. Nanotechnol. **5**, 160 (2010).

[60] G. Maglia, M. R. Restrepo, E. Mikhailova, and H. Bayley, Proc. Natl. Acad. Sci. USA **105**, 19720 (2008).

[61] D. Branton *et al.*, Nat. Biotechnol. **26**, 1146 (2008).

[62] R. Marie, J. N. Pedersen, L. Bærlocher, K. Koprowska, M. Pødenphant, C. Sabatel, M. Zalkovskij, A. Mironov, B. Bilenberg, N. Ashley, H. Flyvbjerg, W. F. Bodmer, A. Kristensen, and K. U. Mir, Proc. Natl. Acad. Sci. USA **115**, 11192 (2018).

[63] S. Jin and L. R. Collins, New J. Phys. **9**, 360 (2007).

[64] J. D. Weeks, D. Chandler, and H. C. Andersen, J. Chem. Phys. **54**, 5237 (1971).

[65] R. Zwanzig, *Nonequilibrium Statistical Mechanics* (Oxford University Press, Oxford, UK, 2001)

[66] M. Doi and S. F. Edwards, *The Theory of Polymer Dynamics* (Oxford University Press, Oxford, UK, 1988), Vol. 73.

[67] F. Weik, R. Weeber, K. Szuttor, K. Breitsprecher, J. de Graaf, M. Kuron, J. Landsgesell, H. Menke, D. Sean, and C. Holm, Eur. Phys. J. Spec. Top. **227**, 1789 (2019).

[68] I. Huopaniemi, K. Luo, T. Ala-Nissila, and S.-C. Ying, J. Chem. Phys. **125**, 124901 (2006).

[69] A. Gopinathan and Y. W. Kim, Phys. Rev. Lett. **99**, 228106 (2007).

[70] W.-P. Cao, L.-Z. Sun, C. Wang, and M.-B. Luo, J. Chem. Phys. **135**, 174901 (2011).

[71] J. Elgeti and G. Gompper, Eur. Phys. J. Spec. Top. **225**, 2333 (2016).

[72] K. Schaar, A. Zöttl, and H. Stark, Phys. Rev. Lett. **115**, 038101 (2015).

[73] M. C. Marchetti, Y. Fily, S. Henkes, A. Patch, and D. Yllanes, Curr. Opin. Colloid Interface Sci. **21**, 34 (2016).

[74] M. Zarif and A. Naji, Phys. Rev. E **102**, 032613 (2020).

[75] M. Sebtosheikh and A. Naji, Sci. Rep. **11**, 23100 (2021).

[76] M. Sebtosheikh and A. Naji, arXiv:2208.07615.

[77] A. Torrik, A. Naji, and M. Zarif, Phys. Rev. E **104**, 064610 (2021).

[78] B.-q. Ai, Z.-g. Shao, and W.-r. Zhong, Soft Matter **14**, 4388 (2018).

[79] B. Liebchen and D. Levis, Phys. Rev. Lett. **119**, 058002 (2017).

[80] H. Löwen, Eur. Phys. J. Spec. Top. **225**, 2319 (2016).

[81] T. Jamali and A. Naji, Soft Matter **14**, 4820 (2018).

[82] Z. Fazli and A. Naji, Phys. Rev. E **103**, 022601 (2021).

[83] T. Narayanan and A. Kumar, Phys. Rep. **249**, 135 (1994).

[84] K. Luo, S. T. T. Ollila, I. Huopaniemi, T. Ala-Nissila, P. Pomorski, M. Karttunen, S.-C. Ying, and A. Bhattacharya, Phys. Rev. E **78**, 050901(R) (2008).

[85] C. T. A. Wong and M. Muthukumar, Biophys. J. **95**, 3619 (2008).

[86] M.-A. Paun, V.-A. Paun, and V.-P. Paun, Polymers **14**, 2090 (2022).

[87] A. Carollo, D. Valenti, and B. Spagnolo, Phys. Rep. **838**, 1 (2020).

[88] A. V. Yakimov, D. O. Filatov, O. N. Gorshkov, D. A. Antonov, D. A. Liskin, I. N. Antonov, A. V. Belyakov, A. V. Klyuev,

[89] A. Carollo, and B. Spagnolo, Appl. Phys. Lett. **114**, 253506 (2019).

[89] C. Guarcello, D. Valenti, A. Carollo, and B. Spagnolo, Entropy **17**, 2862 (2015).

[90] A. Carollo, B. Spagnolo, A. A. Dubkov, and D. Valenti, J. Stat. Mech. (2019) 094010.

[91] Y. V. Ushakov, A. A. Dubkov, and B. Spagnolo, Phys. Rev. E **81**, 041911 (2010).

[92] N. V. Agudov, A. V. Safonov, A. V. Krichigin, A. A. Kharcheva, A. A. Dubkov, D. Valenti, D. V. Guseinov, A. I. Belov, A. N. Mikhaylov, A. Carollo, and B. Spagnolo, J. Stat. Mech. (2020) 024003.

[93] A. Mikhaylov, D. Guseinov, A. Belov, D. Korolev, V. Shishmakova, M. Koryazhkina, D. Filatov, O. Gorshkov, D. Maldonado, F. Alonso, J. Roldán, A. Krichigin, N. Agudov, A. Dubkov, A. Carollo, and B. Spagnolo, Chaos Solitons Fract. **144**, 110723 (2021).

[94] N. Pizzolato, A. Fiasconaro, and B. Spagnolo, Int. J. Bifurcation Chaos **18**, 2871 (2008).

[95] D. Valenti, G. Denaro, D. Adorno, N. Pizzolato, S. Zammito, and B. Spagnolo, Cent. Eur. J. Phys. **10**, 560 (2012).

[96] M.-B. Luo, F. Wu, S. Zhang, and L.-Z. Sun, Mol. Simul. **45**, 1044 (2019).

[97] N. Pizzolato, A. Fiasconaro, and B. Spagnolo, J. Stat. Mech. (2009) P01011.

[98] P. J. Park and W. Sung, Int. J. Bifurcat. Chaos **08**, 927 (1998).

[99] N. Pizzolato, A. Fiasconaro, D. P. Adorno, and B. Spagnolo, Phys. Biol. **7**, 034001 (2010).

[100] D. Mondal and M. Muthukumar, J. Chem. Phys. **144**, 144901 (2016).

[101] N. Pizzolato, A. Fiasconaro, D. P. Adorno, and B. Spagnolo, J. Chem. Phys. **138**, 054902 (2013).

[102] T.-C. Lee, M. Alarcon-Correa, C. Miksch, K. Hahn, J. G. Gibbs, and P. Fischer, Nano Lett. **14**, 2407 (2014).

[103] D. A. Wilson, R. J. M. Nolte, and J. C. M. van Hest, Nat. Chem. **4**, 268 (2012).

[104] D. Takagi, A. B. Braunschweig, J. Zhang, and M. J. Shelley, Phys. Rev. Lett. **110**, 038301 (2013).

[105] D. Takagi, J. Palacci, A. B. Braunschweig, M. J. Shelley, and J. Zhang, Soft Matter **10**, 1784 (2014).

[106] M. S. D. Wykes, X. Zhong, J. Tong, T. Adachi, Y. Liu, L. Ristroph, M. D. Ward, M. J. Shelley, and J. Zhang, Soft Matter **13**, 4681 (2017).